48th AIAA Aerospace Sciences Meeting Including the New Horizons Forum and Aerospace Exposition
4 - 7 January 2010, Orlando, Florida
AIAA 2010-1432

Shape Optimization and Fluid Dynamic Analysis of a Translating Flexible Body

Scott L. Thomson[1]
Brigham Young University, Provo, UT, 84663

The translation (swimming) of an oscillating, slender, flexible body through an initially stationary fluid was explored using computational models and optimization routines. The computational model included fully-coupled two-dimensional fluid and solid finite element domains. The body leading edge was subjected to a prescribed vertical sinusoidal displacement, whereas the entire body was free to move horizontally. Large body deformation resulted in thrust production and horizontal body translation. Gradient-based optimization methods were used to find the body shape that yielded the maximum horizontal displacement over one period of vertical oscillation. It is shown that a tapered body with a "rounded" leading edge achieved significantly greater horizontal velocity than a body of uniform thickness. The computational domains, numerical models, optimization routines, and model verification studies are described. The predicted responses of uniform and optimal bodies are compared, and the sensitivity of horizontal displacement to body shape is quantified.

I. Introduction

The purpose of this paper is to explore the response of an optimized slender body translating ("swimming") through an initially stationary fluid. The research is motivated by previous experimental studies of propulsion generated by flapping motion. A review of the literature on this topic is not attempted here. Among the most relevant include studies on a sinusoidally pitching and plunging airfoil[1], a sinusoidally-plunging airfoil with a flexible trailing edge[2], and an oscillating fin[3].

Heathcote and Gursul[2] performed experiments on a rigid airfoil with a very thin plate attached to the trailing edge. Various plate thicknesses were studied and the presence of an optimal thickness for thrust coefficient generation was noted, although identification of a truly "optimal" configuration was not the goal of the study.

In the present paper, a computational model of a body translating through a fluid is presented. The model included separate, but coupled, fluid and solid domains. Combinations of sliding and deforming meshes allowed for large fluid and solid domain displacements. Verification studies were performed to explore sensitivity to grid size and time step size. The model was coupled with optimization routines to search for the optimal shape for maximizing horizontal displacement. The purpose of the optimization algorithm was not for design; but rather, it was intended to be used as an efficient tool for exploring the parameter space, from which further models may be investigated in more detail.

II. Numerical Methods

A. Coupled Fluid-Solid Model

Fully-coupled fluid and solid domains were modeled in two dimensions using the finite element method with the commerical code ADINA (ADINA R&D, Inc., Watertown, MA). The fluid domain was governed by the unsteady, incompressible, viscous Navier-Stokes equations. The modeled fluid was water (ρ_{fluid} = 1000 kg/m^3, μ = 0.001 Pa·s). A laminar flow model was used. The solid domain was based on the large deformation of a linearly-elastic steel material model (ρ_{solid} = 7861 kg/m^3, E = 210 GPa, ν = 0.3). The solid domain was 0.09 cm long and was of variable thickness, as discussed below. The fluid domain dimensions and boundary conditions are noted in Fig. 1. No external fluid forces were applied; thus the only fluid motion was that which resulted from motion of the solid body.

[1]Assistant Professor, Mechanical Engineering, 435 CTB, AIAA Member.

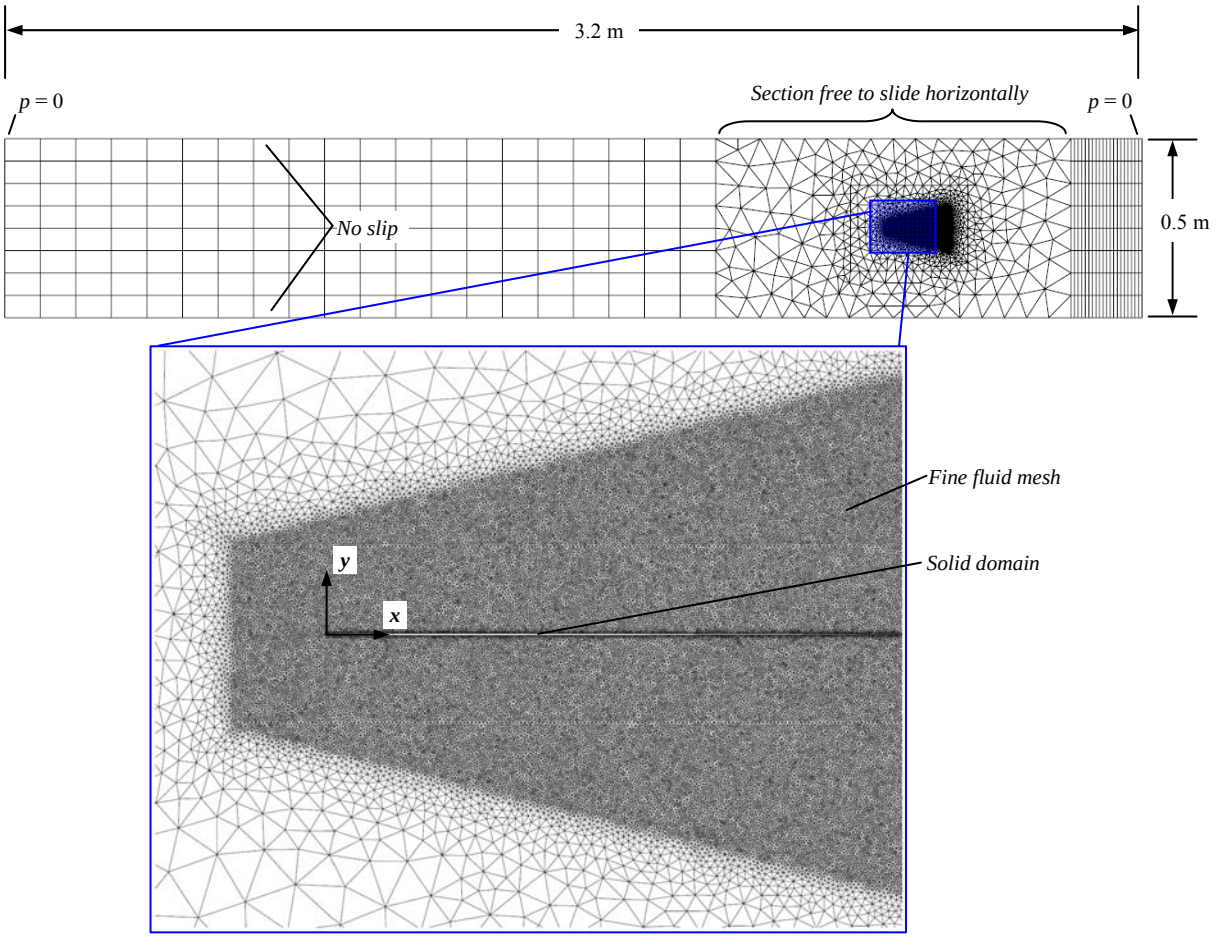

Figure 1. Computational fluid domain grid. Also visible is the upstream, unmeshed portion of the solid domain. The fluid grid shown here has 1.25×10^{-4} m element spacing adjacent to the solid domain boundary and a total of 149,885 nodes and 297,880 elements (see Fig. 5).

The solid body was completely immersed in the fluid. The boundary conditions along the fluid-solid interface enforced consistent displacement of the fluid and solid domains, and equal stresses along the fluid-solid interface. A prescribed sinusoidal vertical motion with an amplitude of 1.746×10^{-2} m and a frequency of 0.9753 Hz was applied to the leading edge of the solid domain at $x = 0$ (see coordinate system definition in Fig. 1). This resulted in horizontal thrust production, which in turn generated horizontal motion of the solid body in the $-x$ direction. The fluid mesh in the immediate proximity of the solid domain deformed along with the body. A larger fluid mesh section was allowed to slide horizontally (see Fig. 1). This combination of mesh movements allowed for significant body motion, as described below. Verification studies were performed to identify grid-independent and time step size-independent parameters.

B. Optimization Strategy

Optimization was used to find the body shape that led to the maximum horizontal displacement after one period of vertical oscillation (T = 1.0253 sec). The commercial code MATLAB, coupled with ADINA, was used to guide the optimization search. Optimization proceeded according to the following steps:

(1) Preliminary (trial) gradient-based optimization runs were performed with a 0.09 m-long plate. The plate thickness at 11 uniformly-spaced points along the body x-dimension was varied throughout the optimization. The body length remained unchanged. The minimum and maximum thickness constraints in this portion of the study were 20 μm and 2000 μm, respectively.

(2) Trial shapes from Step (1) were input into a genetic algorithm (GA) to facilitate a broader parameter search. Minimum and maximum thickness limits in this portion were 20 μm and 800 μm, respectively.

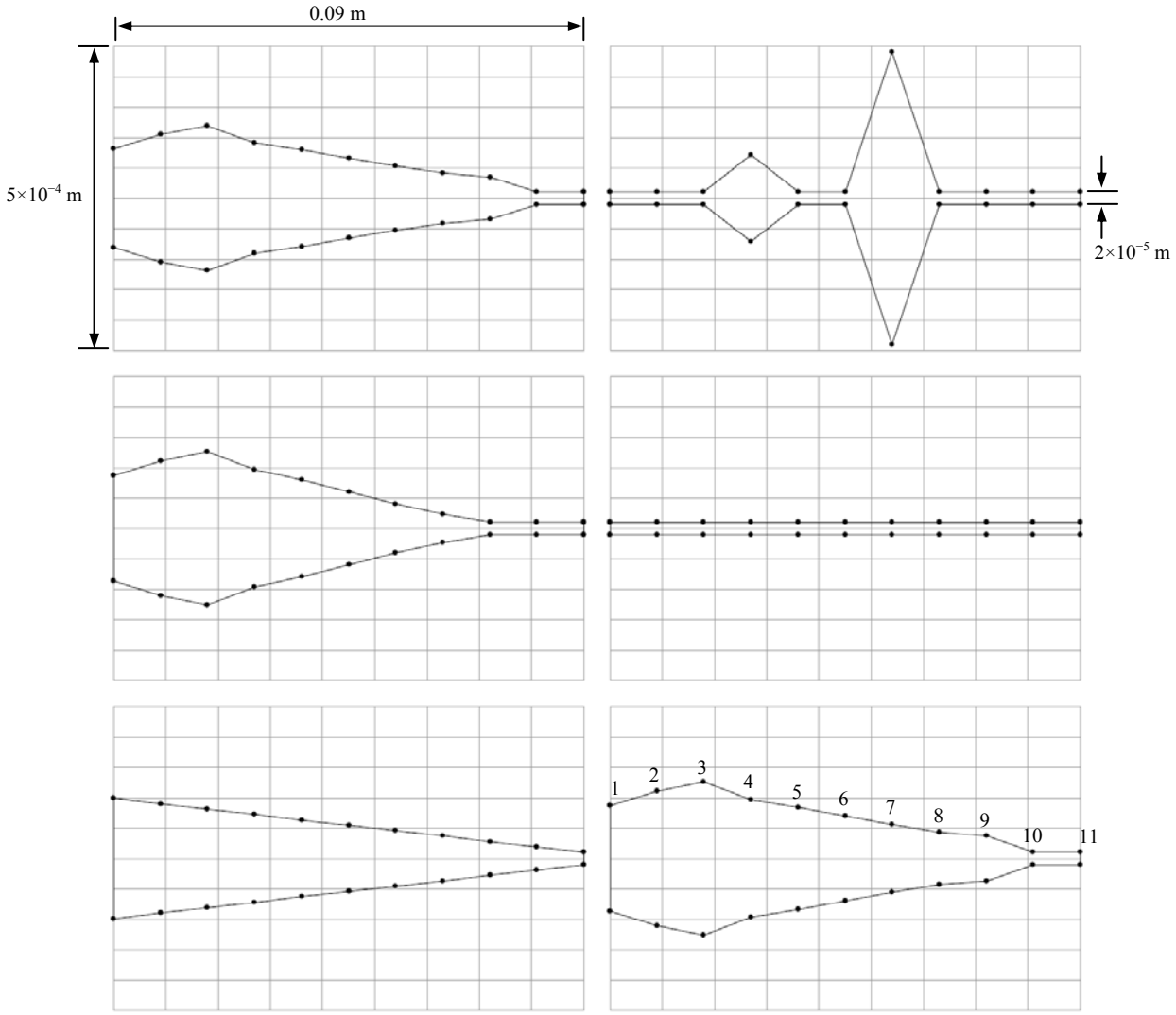

Figure 2. Six of the initial shapes input into the genetic algorithm. Horizontal and vertical dimensions are not to scale; refer to the provided dimensions for accurate scaling. Numbered control points defining body thickness are shown in the lower right shape.

The population size was 22. Figure 2 shows six of the initial population shapes; the remaining 16 were randomly assigned. Note that, for visibility, the *y*-axis of the plots in Fig. 2 has been significantly stretched.

(3) A gradient optimization search was performed using the genetic algorithm-derived shape from Step (2).

(4) As a check, a final gradient optimization search was performed using the optimal shape from Step (3).

III. Results

A. Numerical Validation

Preliminary validation of the ADINA fluid-structure interaction code was accomplished by simulating one of the experimental studies of Heathcote and Gursul[2]. The case was that of a teardrop-shaped airfoil segment with a thin plate attached to the airfoil segment trailing edge, as shown in Fig. 3. This was performed using similar fluid and solid domains as shown in Fig. 1, although in this case, horizontal motion was not allowed. Vertical plunging motion of the airfoil segment was prescribed according to the equation $y = A\sin(2\pi ft)$, where A = 1.746 cm and f = 0.9753 Hz. The ADINA solid domain was defined using a material with a modulus of 210 GPA and a density of 7861 kg/m^3. The teardrop-shaped airfoil segment was 3 cm long and 1 cm thick at the widest point. Attached to the airfoil trailing edge was a thin plate (or sheet in 2D), with thickness 50.4 μm and the same material properties as the

leading segment. The fluid domain was modeled as water (ρ = 1000 kg/m^3, μ = 0.001 Pa.s). Fluid domain inlet flow velocity was 0.1 m/s. The Reynolds number, Re = $\rho Uc/\nu$ (based on U = 0.1 m/s, c = 0.09 m), was 9000. The Strouhal number, St = $2Af/U$ (based on A = 0.01746 cm, f = 0.9753 Hz, U = 0.1 m/s), was 0.34. A laminar flow solver was used.

Leading and trailing edge displacement data are shown in Fig. 4. The predicted trailing edge displacement data are within approximately 10% of experimental data (see Fig. 16 of Heathcote and Gursul[2]). This agreement is acceptable, although further model validation (e.g., thrust coefficient, velocity field data) is necessary.

B. Numerical Verification

We now return to the original problem set up in Sec. II, in which the model was allowed to translate horizontally. The sensitivity of the model displacement to grid size (via grid doubling) and time step size (via factor of 10 decrease in time step size) was examined. The results are shown in Fig. 5. The negative x-displacement indicates leftward motion of the model as oriented in Fig. 1.

The model converged towards a consistent result with finer grid sizes, and is relatively insensitive to time step size beyond dt = 0.02 sec. Grid sizes are summarized in Table 1. Because of the computational cost of running thousands of transient simulations in the optimization studies, the coarsest mesh was employed in optimization. It is acknowledged that while this grid yielded qualitatively similar results than the fine grid, the quantitative displacement differed significantly. Further studies into the influence of grid size on optimization outcome would be of interest.

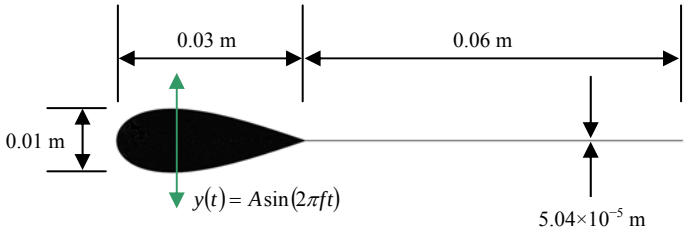

Figure 3. Teardrop-shaped airfoil segment with flexible trailing edge, modeled after Heathcote and Gursul[2], used for numerical model validation.

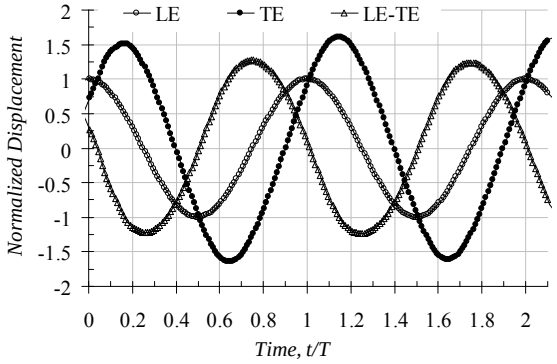

Figure 4. Displacement (normalized by prescribed input displacement amplitude, A) vs. time as predicted by numerical model. Shown are leading edge (LE), trailing edge (TE), and (LE − TE) displacements.

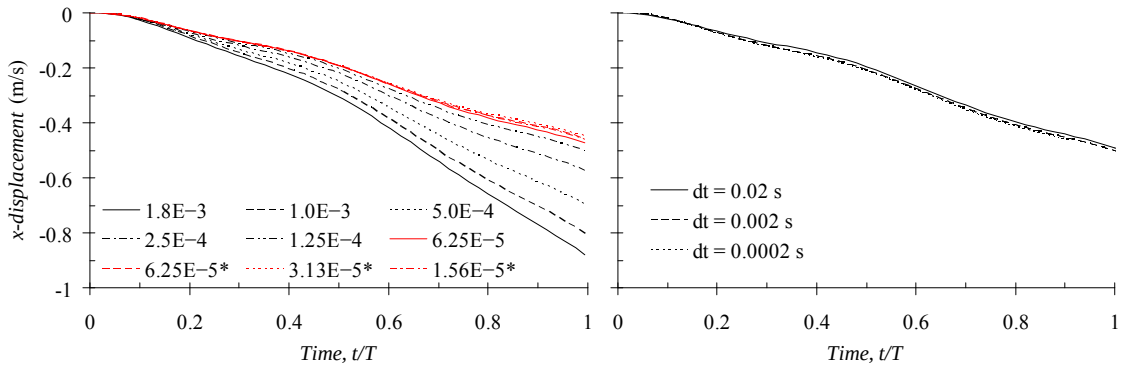

Figure 5. Horizontal (*x*) displacement vs. time using different grid densities (left) and time step sizes (right). The left plot legend denotes distance between adjacent nodes in the fluid domain at the fluid-solid interface. See Table 1 for further details.

Table 1. Number of nodes and elements for grid refinement study. Asterisks denote cases where, for computational efficiency, the grid was significantly coarser away from the airfoil surface.

Node spacing (m) along fluid-solid interface	*Total number of nodes*	*Total number of elements*
1.8E−3	1,937	3,324
1.0E−3	4,317	8,004
5.0E−4	12,240	23,670
2.5E−4	41,046	80,922
1.25E−4	149,885	297,880
6.25E−5	574,617	1,145,904
6.25E−5*	31,570	59,808
3.13E−5*	90,061	173,908
1.56E−5*	290,425	568,870

C. Optimization Results

Figure 6 shows the genetic algorithm optimization convergence history. Shown are 363 iterations. Note that each generation consisted of 22 iterations, thus between 16 and 17 generations are shown. The best individual from the first generation resulted in a displacement of −0.878 m in the *x*-direction after one period, whereas the mean displacement of the first generation was −0.525 m. The best individual from the 16th generation translated −0.879 m in the *x*-direction after one period, whereas the 16th generation mean displacement was −0.877 m. The subsequent gradient optimization runs yielded shapes that translated −0.891 m. Therefore, the genetic algorithm yielded a shape that was only a marginal improvement over the initial gradient optimization trial run, but one which was able to be improved upon via subsequent gradient-based optimization.

The final "optimal" shape is shown in Fig. 7. Note that, as with Fig. 2, the *y*-axis has been stretched for visibility. The shape resembles three of the initial population shapes shown in Fig. 2. The shape contains a semi-rounded leading edge, followed by a gradual taper to the trailing edge. It is interesting to note that the taper is not constant (i.e., it does not follow a straight line).

Figure 8 shows images of the grid as it translates with the solid domain. Figure 9 shows images of the optimized body during the first 18% of a period. Shown are images of the body at intervals of $t/T = 0.02$. Deformation of the body (e.g., particularly the "concave up" shape of the trailing edge during the first few time steps), is evident.

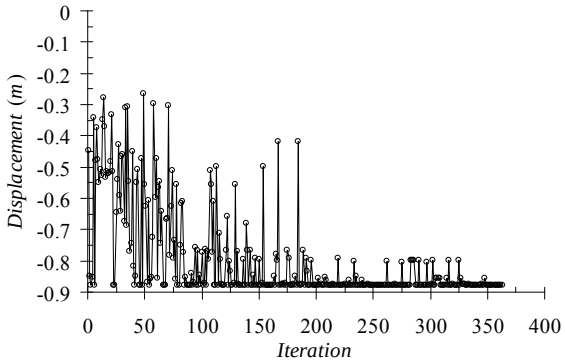

Figure 6. Optimization convergence.

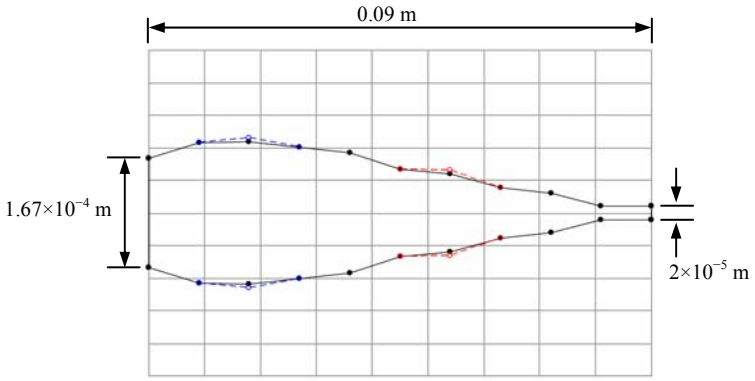

Figure 7. Optimized body shape (black). Blue and red curves denote positive perturbations to the *y*-values of points 3 and 7, respectively, as performed in the sensitivity studies (Sec. D).

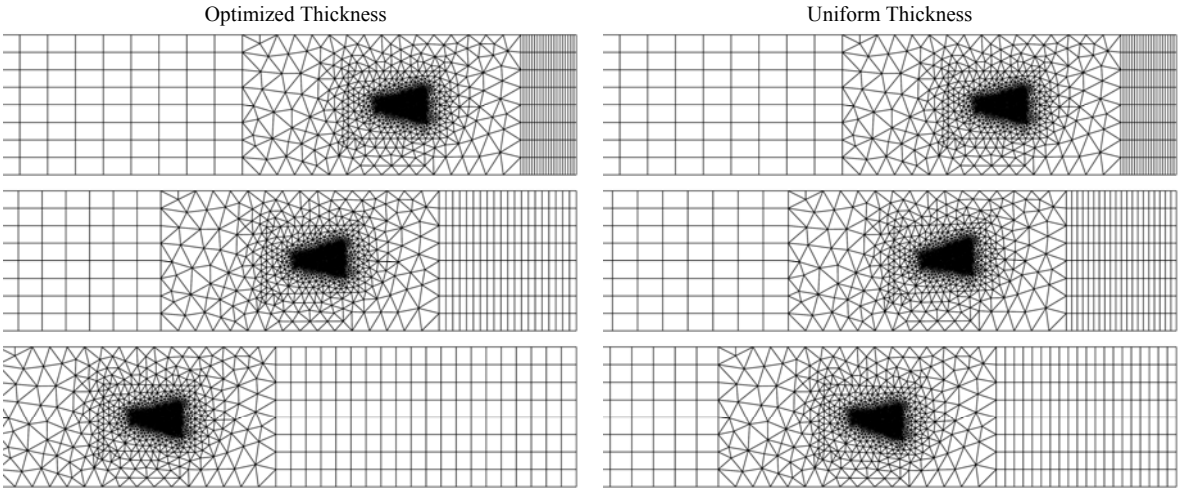

Figure 8. Mesh positions for optimized (left) and uniform (2×10^{-5} m, right) bodies at times t/T = 0, 0.49, and 1.

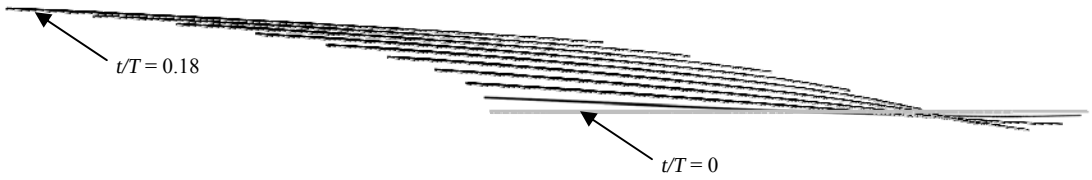

Figure 9. Snapshots of body position at *t/T* = 0.02 intervals from *t/T* = 0 to *t/T* = 0.18.

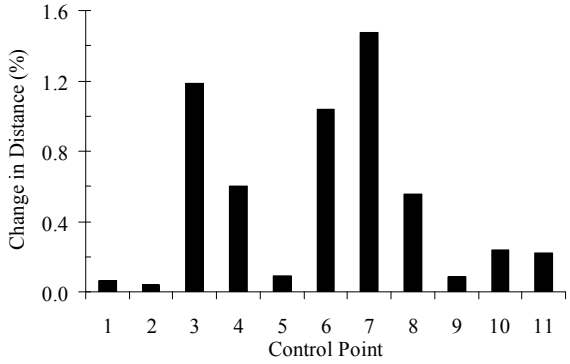

Figure 10. Change in *x*-displacement resulting from each 10 μm perturbation in control point *y*-position, expressed as a percentage of the optimized body displacement.

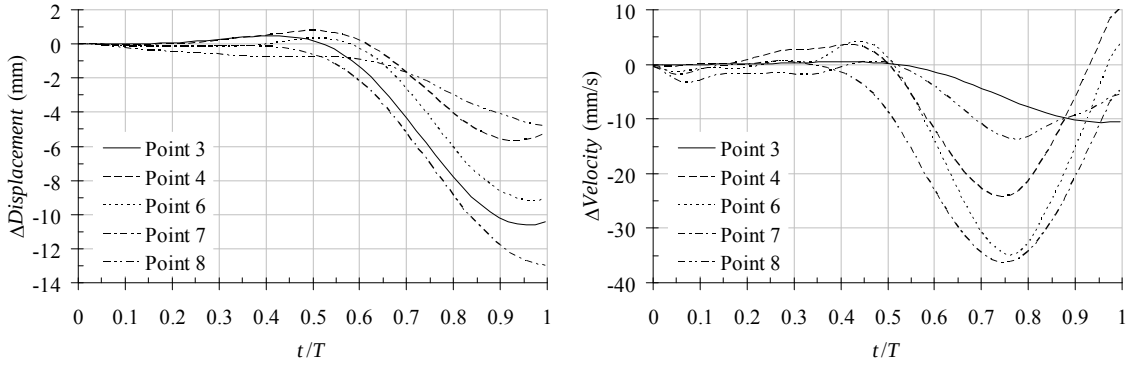

Figure 11. Change in *x*-displacement (left) and change in *x*-velocity (right) vs. time resulting from 10 μm increases in *y*-positions of control points 3, 4, 6, 7, and 8. Displacement and velocity changes are relative to optimized body displacement.

D. Sensitivity Study Results

The sensitivity of the predicted displacement of the optimized body (Fig. 7) was studied by sequentially perturbing the thickness of the body at each control point by a small amount (10 μm). Figure 10 shows that the body translation was most sensitive to changes to point 7, and least sensitive to changes to point 2. Increasing the body thickness by 10 μm at point 7 resulted in a 1.5% decrease in body translation over one period, compared with a 0.04% decrease in translation when the thickness at point 2 was correspondingly increased. Figure 11 shows that this decrease in translation was primarily due to a sharp decrease in velocity after the first half-period. Further investigation is required to determine the cause of this change in velocity. The velocities for all cases over the first half-period were all similar.

IV. Conclusions

The work presented here represents initial results towards optimizing the shape of a "swimming" body. The results illustrate the functionality of an optimization routine coupled with a fluid-solid commercial code. The code allows for large deformation and translation of the solid body and coupled fluid mesh. The motion of the optimized

and uniform body shapes is shown and differences are noted, although further work is necessary in several areas, including further validation with experimental data, development of an understanding of why the optimum shape is optimal, and exploring different optimization criteria, such as power and efficiency. Additionally, it will be important to investigate the influence of grid size on optimization outcome.

References

[1]McGowan, G., Gopalarathnam, A., Ol, M., Edwards, J., Fredberg, D. (2008). "Computation vs. experiment for high-frequency low-Reynolds number airfoil pitch and plunge," AIAA 2008-0653.

[2]Heathcote, S., Gursul, I. (2007). "Flexible flapping airfoil propulsion at low reynolds numbers," *AIAA Journal*, Vol. 45, pp. 1066-1079.

[3]Bandyopadhyay, P. R., Beal, D. N., and Menozzi, A. (2008). "Biorobotic insights into how animals swim," *The Journal of Experimental Biology*, Vol. 211, pp. 206-214.